IVYSPRING INTERNATIONAL PUBLISHER

Theranostics

2017; 7(6): 1531-1542. doi: 10.7150/thno.17247

Research Paper

A New Green Titania with Enhanced NIR Absorption for Mitochondria-Targeted Cancer Therapy

Juan Mou, Tianquan Lin, Fuqiang Huang, Jianlin Shi and Hangrong Chen✉

State Key Laboratory of High Performance Ceramics and Superfine Microstructure, Shanghai Institute of Ceramics, Chinese Academy of Sciences, Shanghai 200050, P. R. China.

✉ Corresponding author: hrchen@mail.sic.ac.cn

Received: 2016.08.18; Accepted: 2017.01.06; Published: 2017.04.07

Abstract

A new kind of green titania (*G*-TiO_{2-x}) with obvious green color was facilely synthesized from black titania (*B*-TiO_{2-x}) through subsequently strong ultrasonication. Comparatively, this stable *G*-TiO_{2-x} shows much enhanced near infrared (NIR) absorption, especially around 920 nm, which can be ascribed to the obvious change of TiO_{2-x} lattice order owing to the effect of ultrasonication. This feature enables *G*-TiO_{2-x} to be stimulated with 980 nm laser in the combined photodynamic therapy (PDT) and photothermal therapy (PTT), which is greatly beneficial for improving tissue penetration depth. Furthermore, since mitochondria are preferred subcellular organelles for PDT/PTT, *G*-TiO_{2-x} was further designed to conjugate with triphenylphosphonium (TPP) ligand for mitochondria-targeted PDT/PTT to obtain precise cancer treatment. Attributing to the high mitochondria-targeting efficiency and simultaneously synergistic PDT/PTT, high phototherapeutic efficacy and safety with a much lower laser power density (980 nm, 0.72 W cm^{-2}) and low materials dosage were achieved both *in vitro* and *in vivo*. In addition, negligible toxicity was found, indicating high biocompatibility. This novel *G*-TiO_{2-x} could provide new strategies for future precise minimal/non-invasive tumor treatment.

Key words: green titania, NIR absorption, mitochondria, photodynamic therapy, photothermal therapy.

Introduction

Over the past decades, breakthroughs in phototherapy including photothermal therapy (PTT) [1] and photodynamic therapy (PDT)[2] have ushered new frontiers in cancer treatment. PTT involves the administration of photosensitizers to effectively convert light energy into hyperthermia inducing cancer cells death. While, PDT employs photosensitizers to produce toxic reactive oxygen species (ROS) for cancer cells destruction, which has emerged as a site specific treatment modality of disease. However, both of them still have many challenges or series of limitations, such as oxygen dependence, high administration dose and less efficient treatment efficacy of PDT, as well as non-selectivity, risk of damaging neighboring normal tissues and requirement of high laser power density of PTT, *etc.* Synergetic tumor phototherapy could be achieved if these two modalities are combined, due to the differences in cell-killing mechanism and overcoming respective limitation [3, 4]. Currently, a number of PTT agents such as gold nanostructures [5-7], nano-graphene oxide [8, 9], *etc.*, conjugated with various PDT photosensitizers, such as Ce6, methylene blue, indocyanine green (ICG), and phthalocyanine, *etc.*, have been administrated in the combinatorial phototherapy of PDT and PTT, and achieved synergistic cancer treatment. However, such nanocomposites generally suffer from the requirement of two lasers with different wavelengths to excite PDT and PTT, respectively, which is due to the absorption mismatch of different functional components. In addition, multicomponents may induce inevitable systemic side effects and toxicity. Therefore, it is highly desired but challenging to

develop a single component nanomaterial and enable it to obtain the simultaneous PDT and PTT under the same single laser irradiation.

Titania, as one of the most common commercial and widely used functional materials, has triggered intensive interests in the fields of solar energy conversion, environmental remediation, and biomedical application [10-13]. Attributing to its excellent photocatalytic property, low toxicity and high photostability, titania is capable of generating various cytotoxic ROS (*e.g.*, $OH^{\bullet}$, $O_2^{\bullet-}$, H_2O_2) [14-16], which can result in severe cancer cells death, and has been regarded as a favorable candidate for PDT [17]. However, its overall phototherapeutic efficacy for PDT is much limited by ultraviolet (UV) light (λ=275–390 nm), inducing side effects to healthy tissues and shallow penetration [18]. Comparatively, NIR laser (λ=700–1300 nm), locating in biological transparency window [19, 20], is preferable for phototherapy due to its lower energy and deeper tissue penetration. Therefore, many efforts have been proposed to extend the optical response of titania from UV to visible and NIR region, such as doping and introducing metal (*e.g.*, Fe, Ag, Pt, Zr, *etc.*) [21], non-metal (*e.g.*, B, C, N, F, P, S, *etc.*) elements [22, 23], and self-doping methods [24-26], *etc.*. For example, the recently discovered black titania nanoparticles [27-30] have opened new avenues to broaden their optical absorption from UV to NIR region to some extent, and triggered explosive interests in energy and biological fields. However, attributing to its limited absorption in NIR region, the laser power density generally used for PTT is as high as 2 W cm^{-2} [31], which exceeds the conservative limit (*i.e.*, 0.33 W cm^{-2} with 808 nm laser irradiation [32]; 0.72 W cm^{-2} with 980 nm laser irradiation [33]) and has potential damages to the neighboring normal tissues. Therefore, the therapeutic efficacy and safety of titania for PDT and PTT are needed to be improved.

Very recently, mitochondria-targeted PTT [34] and PDT [35, 36] have emerged as new strategies for improving therapeutic efficiency and safety, since mitochondria are vital energy-producing cellular organelles and highly susceptible to heat shock [37], generally resulting in apoptotic cell death through the generation of ROS [38]. Thus we believe the combination of mitochondria-targeted PDT and PTT will bring preferable outcomes regarding to circumventing their respect limitations, reducing laser power density and materials dosage.

Herein, we reported a simple and effective method to construct a new kind of self-doped green titania (*G*-TiO_{2-x}) with enhanced NIR absorption, and explored its potential biomedical application in cancer phototherapy. This stable *G*-TiO_{2-x} could be facilely and irreversibly synthesized from black titania (*B*-TiO_{2-x}) by subsequently strong ultrasonication. The aqueous solution containing *G*-TiO_{2-x} displayed an obvious green color and enhanced NIR absorption, especially around 920 nm. This significant enhancement in NIR absorption enables this new *G*-TiO_{2-x} to act as an excellent single NIR laser-induced photosensitizer for combined PDT and PTT. In order to further reduce the laser power density, minimize side effects, and improve the phototherapeutic efficacy, *G*-TiO_{2-x} was subsequently conjugated with triphenylphosphonium (TPP), which is a cation selectively accumulating within energized mitochondria [39], to construct a novel mitochondria-targeted nanoplatform for precise cancer treatment. Both *in vitro* and *in vivo* results well demonstrated the capability of *G*-TiO_{2-x} with TPP functionalization (*G*-TiO_{2-x}-TPP) for simultaneously mitochondria-targeting and synergistic PDT/PTT, under a single NIR laser irradiation at a much lower laser power density (980nm, 0.72 W cm^{-2}) and low dosage. This new *G*-TiO_{2-x} will open broad horizons for the explorations of titania-based and subcellular organelle-specific nanomaterials for further precise cancer treatment.

Materials and Methods

Chemicals and Reagents

All reagents were used without further purification. N-(3-Dimethylaminopropyl)-N-ethylcarbodiimide hydrochloride (EDC, 98%), N-(4-Chloro-3-trifluoromethyl-phenyl)-2-ethoxy-benz amide (CTPB, 98%), Rhodamine B isothiocyanate (RITC) were purchased from Sigma-Aldrich. Amine polyethylene glycol amine (H_2N-PEG_{5000}-NH_2, MW=5000) was purchased from JenKem Technology Co., Ltd (Beijing, China). 1, 3-diphenylisobenzofuran (DPBF), 5, 5-Dimethyl-1-pyrroline-N-oxide (DMPO), 2, 7-dichloro-dihydro-fluorescien diacetate (DCFH-DA), Mito-Tracker Green were purchased from Beyotime Biotechnology Co., Ltd. Dulbecco Modified Eagle Medium (DMEM), Roswell Park Memorial Insitute medium (RPMI) 1640, fetal bovine serum (FBS), penicillin and streptomycin, and cell culture dishes were purchased from Thermo Fisher Scientific (shanghai) Co., Ltd. P25, Al, dimethyl sulfoxide (DMSO) and phosphate buffer solution (PBS) were purchased from Sinopharm Chemical Reagent Co., Ltd. (Shanghai, China).

Preparation of G-TiO_{2-x}

Firstly, pristine *B*-TiO_{2-x} was mass-produced from P25 *via* an aluminum reduction according to previously reported [40]. In a typical procedure, P25 and aluminum were put in a two zone tube furnace,

separately, and then vacuumized to a base pressure lower than 0.5 Pa. Following, aluminum and P25 were subjected to heating at 800 °C and 600 °C for 6 h, respectively. Then, the post-annealing treatment was performed by heating the obtained Al-TiO_{2-x} sample at 800 °C in an argon atmosphere for 12 h. After that, *B*-TiO_{2-x} was prepared and then dispersed in water with ultrasonication at 400 W for 2 h at room temperature. Finally, highly dispersible aqueous solution of *G*-TiO_{2-x} was acquired through this robust and simple way.

PEG, TPP and RITC conjugation of G-TiO_{2-x}

In order to conjugate TPP ligand on the surface of *G*-TiO_{2-x}, H_2N-PEG_{5000}-NH_2 was firstly linked to *G*-TiO_{2-x} for anchoring site. Briefly, to the aqueous solution of *G*-TiO_{2-x} (Ti concentration: 1 mg mL^{-1}), excess H_2N-PEG_{5000}-NH_2 (5-10 mg) was added and the mixture was stirred at room temperature for 24 h. *G*-TiO_{2-x}-NH_2 was obtained after centrifugation (11000 rpm, 15 min) and freeze-dried for later use. As for TPP conjugation, EDC (50 mg) and CTPB (20 mg) were dissolved in 20 mL of methanol. Thereafter, *G*-TiO_{2-x}-NH_2 (1 mg mL^{-1}) was added to the abovementioned mixture solution and strirred at room temperature for 24 h. Finally, *G*-TiO_{2-x}-TPP was obtained after centrifugation (11000 rpm, 15 min) and washed for several times, then dispersed in water for later use (0.5 mg mL^{-1}).

RITC was conjugated on the surface of *G*-TiO_{2-x}-NH_2 and *G*-TiO_{2-x}-TPP for fluorescent labeling. Briefly, to the aqueous solutions of *G*-TiO_{2-x}-NH_2 and *G*-TiO_{2-x}-TPP (1 mg mL^{-1}), excess RITC (2-5 mg) was added and the mixtures were stirred at room temperature for 24 h. RITC can be attached on the surface of *G*-TiO_{2-x}-NH_2 and *G*-TiO_{2-x}-TPP by forming thiourea linkage between NH_2 originating from *G*-TiO_{2-x}-NH_2 and *G*-TiO_{2-x}-TPP and S=C=N group originating from RITC, respectively. RITC labeled *G*-TiO_{2-x}-NH_2 and *G*-TiO_{2-x}-TPP were obtained after centrifugation (11000 rpm, 15 min) and washed for several times, then dispersed in water for later use (0.5 mg mL^{-1}).

ROS detection by using DPBF

ROS prodcution of *G*-TiO_{2-x} (Ti concentration: 100 ppm) was measured by using the sensitive probe DPBF (25 μM) in acetonitrile. A UV-vis absorption spectrum was obtained after every 10 min of NIR (980 nm, 0.72 W cm^{-2}) laser irradiation. The experiment was performed in triplicate and data show as mean ± SD. The monitored absorption decrease of DPBF at 410 nm was ascribed to the consequence of ROS generation.

ESR measurements

5, 5-Dimethyl-1-pyrroline-N-oxide (DMPO, 100 mM, 40 μL), which was used for trapping hydroxyl radicals ($OH^{\bullet}$), was added to the aqueous solotion of *G*-TiO_{2-x} (Ti concentration: 100 ppm). The mixture was irradiated with or without NIR (980 nm, 0.72 W cm^{-2}) laser and then poured into a quartz capillary for the ESR measurement.

Intracellular ROS generation by CLSM

In brief, HeLa cells were seeded on culture dishes (Gibco) at a density of 1 × 10^4 cells mL^{-1} in DMEM, containing 10% FBS and 1% antibiotic solution (penicillin and streptomycin). And incubated with *G*-TiO_{2-x} (Ti concentration: 50 ppm) for cell uptake after 12 h. Then the culture medium was removed and fresh medium containing DCFH-DA (20 μM), which can be transformed into highly fluorescent 2,7-dichlorofluorescein (DCF) in the presence of ROS, was added to the culture dishes for another 30 min incubation. Then the medium containing DCFH-DA was replaced with phosphate buffer solution (PBS) and the cells underwent laser irradiation (980 nm, 0.72 W cm^{-2}, 5 min) for confocal fluorescent imaging. The excitation and emission wavelengths of DCF (green fluorescence) are 485 nm and 530 nm, respectively.

Cell culture

HeLa cells, renal tubular duct epithelial cells of rat (NRK-52E), human glioblastoma cells (U87MG) and rat adrenal pheochromocytoma cell line (PC12) were cultured in a Dulbecco's modified Eagle's medium (DMEM), containing 10% fetal bovine serum and 1% antibiotic solution (penicillin and streptomycin), and maintained at 37 °C under 5% CO_2. Rat liver cells (BRL) and brain capillary endothelial cells (BCECs) were suspended to a standard culture medium containing Roswell Park Memorial Insitute medium (RPMI) 1640, 10% fetal bovine serum, and 1% antibiotic solution and cultured at 37 °C with atmosphere of humidified 5% CO_2.

Intracellular localization of G-TiO_{2-x} and G-TiO_{2-x}-TPP

HeLa cells were seeded on culuture dishes (Gibco) containing DMEM supplemented with 10% FBS and 1% antibiotic solution (penicillin and streptomycin) at a density of 1 × 10^4 cells mL^{-1}, and incubated with RITC-labled *G*-TiO_{2-x} and *G*-TiO_{2-x}-TPP (Ti concentration: 50 ppm) for 1 and 4 h at 37 °C in the presence of 5% CO_2, respectively. Then cells were washed with PBS, Mito-Tracker green (0.1 mM) was added and incubated for another 30 min. Finally, the cells were washed with PBS for 3 times

and imaged by CLSM. The excitation and emission wavelengths of RITC (red fluorescence) are 570 nm and 595 nm, respectively. The excitation and emission wavelengths of Mito-Tracker green (green fluorescence) are 490 nm and 516 nm, respectively.

Photothermal effect of G-TiO_{2-x} solution

To investigate the photothermal effect of *G*-TiO_{2-x} exposured to NIR irradiation, pure water and aqueous solutions (2 mL) containing *G*-TiO_{2-x} at various Ti concentrations (*i.e.*, 6.25, 12.5, 25, 50 ppm) were put in quartz cuvettes and subjected to 980 nm laser irradiation for 5 min at different power densities (*i.e.*, 0.175, 0.35, 0.53, 0.72, 0.89, 1.06 W cm^{-2}). A thermocouple microprobe was inserted into the aqueous solution of *G*-TiO_{2-x} to monitor the temperature change. Meanwhile, the photothermal stability study was performed by irradiating the same aqueous solution of *G*-TiO_{2-x} (2 mL, Ti concentration: 50 ppm) for 10 cycles (980 nm, 0.72 W cm^{-2}, 5 min).

Cytotoxicity evaluation of G-TiO_{2-x}

For the cytotoxicity assay (MTT), cells were seeded in a 96-well plate overnight. Then the original culture medium was repalced by fresh medium containg different Ti concentrations (*i.e.*, 6.25, 12.5, 25, 50, 100 ppm) of *G*-TiO_{2-x}. Then the culture medium was removed and replaced by fresh medium supplement with MTT (8 mg/mL) after aditional 24 h incubation. MTT-formazan dye was formed after 4 h incubation and dissolved by DMSO (100 μL). Finally, the absorbance was measured at A_{490} on an enzyme-linked immuno sorbent assay (ELISA) reader. The test was carried out independently for three times.

In vitro phototoxicity by MTT

Prior to investigate the photodestruction on cancer cells by MTT, HeLa cells were seeded in 96-well cell culture plates (1×10^4 cells per well) for 24 h to adhere and then a series of concentrations of *G*-TiO_{2-x} solution were added for additional 4 h incubation. Following, each well of cells were exposured to 980 nm laser irradiation (0.72 W cm^{-2}, 5 min) and the photo-cytotoxicity study of *G*-TiO_{2-x} was evaluated by the standarded MTT viability assay.

In vitro phototoxicity by trypan blue stain

HeLa cells were seeded on a cell culture plates at 37 °C with 5% CO_2 until reaching 80–90% confluence. Then, original culture medium was replaced with culture medium containing *G*-TiO_{2-x} (Ti concentration: 50 ppm) and incubated for another 4 h. Then cells were illuminated with 980 nm laser (0.72 W cm^{-2}, 5 min). Finally, trypan blue (4%) was used to stain the cells for optical microscopic observation.

In vitro phototoxicity by CLSM

Generally, HeLa cells were incubated in culture dishes at 37 °C in the presence of humidified 5% CO_2 until reaching 80–90% confluence. Then the culture medium containing *G*-TiO_{2-x} (Ti concentration: 50 ppm) was added to replace the original medium for another 4 h incubation. Subsequently, the culture medium was removed and PBS solution was added and followed by 980 nm laser irradiation (0.72 W cm^{-2}, 5 min). After laser irradiation, the cells were co-stained with calcein-AM and PI for confocal fluorescence imaging. The excitation and emission wavelengths of calcein-AM (green fluorescence) are 495 nm and 516 nm, respectively. The excitation and emission wavelengths of PI (red fluorescence) are 535 nm and 617 nm, respectively.

In vivo phototherapeutic efficacy of G-TiO_{2-x}-TPP

In order to evaluate the simultaneous PTT/PDT therapeutic efficacy *in vivo*, nude mice bearing two HeLa tumors on each front flanks were randomly seperated into two groups (n=6): the first and the second groups were treated with saline and PBS solution containing *G*-TiO_{2-x}-TPP (8 mg Kg^{-1}) by tail-vein injection, respectively. Mice were anesthetized prior to 980 nm laser (0.72 W cm^{-2}, 5 min) irradiation on the left flank tumor. The temperature elevation of tumor center during laser irradiation was real-time monitored and recorded on an infrared thermal imaging instrument (FLIR sc325). The tumor size was measured by a digital caliper every 2 days until to 18 days. Tumor volume was calculated by the formula: tumor volume [mm^3] = (length [mm]) × (width [mm])^2 × 0.5, $^*P < 0.05$.

Animal experiments

All animals were purchased and raised at the animal laboratory of Tongji University. All animal experiments were carried out in accordance with the Guidelines for the Care and Use of Research Animals established by Tongji University Animal Studies Committee. HeLa tumor models were established by subcutaneous injection of 1×10^5 cells in 100 μL of PBS into two front flanks of female nude mice. The nude mice bearing HeLa tumors were subjected to phototherapy when volume of tumors reached approximately 100 mm^3. Physiological saline containing *G*-TiO_{2-x}-TPP was intravenously injected into mice.

Statistics

All results in this study are shown as the mean ± SD. Statistical significance with minimum level of P-value set as 0.05 was evaluated by unpaired

two-tailed Student's *t*-test.

Results and Discussions

Synthesis and Characterization

The facile synthesis and rational strategy of such new kind of green titania (*G*-TiO_{2-x}) and TPP functionalized *G*-TiO_{2-x} (*G*-TiO_{2-x}-TPP) for mitochondria-targeted cancer phototherapy, was outlined in **Scheme 1**.

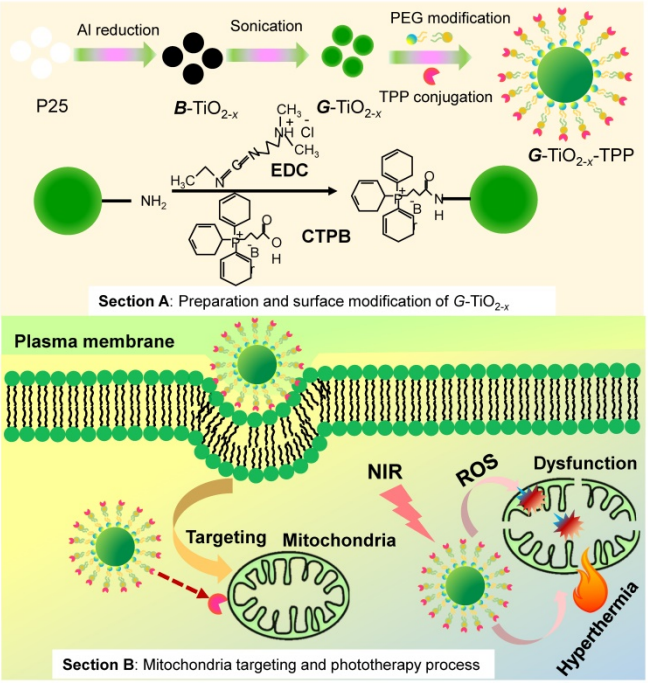

Scheme 1. Schematic representation of the preparation and surface modification of green titania (*G*-TiO_{2-x}) (section A) for mitochondria-targeted cancer phototherapy (section B). Firstly, black titania (*B*-TiO_{2-x}) was synthesized from P25 (pristine titania) through an aluminum reduction method. Then *G*-TiO_{2-x} was prepared from *B*-TiO_{2-x} by strong ultrasonication. The TPP (triphenylphosphonium) was following conjugated to *G*-TiO_{2-x} (*G*-TiO_{2-x}-TPP) for mitochondria targeting strategy. Under the same single near infrared (NIR) laser irradiation, *G*-TiO_{2-x} was able to simultaneously generate reactive oxygen species (ROS) and hyperthermia for photodynamic therapy (PDT) and photothermal therapy (PTT), respectively.

Firstly, black titania (*B*-TiO_{2-x}) with an average particle size of 16 nm (±4 nm) was synthesized through an aluminum reduction method according to previously reported [40]. Then a new kind of *G*-TiO_{2-x} (12.2 ± 2.5 nm) was facilely and irreversibly prepared from *B*-TiO_{2-x} by strong ultrasonication. Both *B*-TiO_{2-x} and *G*-TiO_{2-x} show similar particle size and morphology, as verified by transmission electron microscopy (TEM) in **Figure 1**a and 1c. The size distribution histograms of *B*-TiO_{2-x} and *G*-TiO_{2-x} obtained from the TEM images were shown in Figure S1. All the elements (Ti and O) are obviously detected by energy dispersive spectrometer (EDS) analysis (Figure S2). When dispersed in water, *B*-TiO_{2-x} could quickly precipitate at the bottom of a quartz cuvette (Figure 1b), as the red arrow indicated, suggesting poor dispersity. Comparatively, after strong ultrasonication, the transformed *G*-TiO_{2-x} exhibits an obvious green color and displays excellent dispersity and high stability in water (Figure 1d), mainly attributing to the separation effect of agglomerated NPs induced by ultrasonication and potentially more hydrogen bonds formation between OH groups on the surface and water [41]. The microstructures of *B*-TiO_{2-x} and *G*-TiO_{2-x} were further investigated by high resolution-TEM (HR-TEM). As shown in Figure 1e-f, both *B*-TiO_{2-x} and *G*-TiO_{2-x} are comprised of a highly crystallized TiO_2 core, which shows a well-resolved lattice plane (101) with a typical anatase plane distance, and an amorphous TiO_{2-x} shell. Very interesting, it is noted that apparent thickness enhancement of the disordered outer-layer can be observed after strong ultrasonication (Figure 1e-f), which is attributed to obvious change of TiO_2 lattice order during ultrasonication, inducing the clear formation of amorphous shell around the granula edge [42]. Raman scattering was performed to further examine the structural changes of white TiO_2, *B*-TiO_{2-x} and *G*-TiO_{2-x}. As shown in Figure S3, the six Raman-active modes ($3E_g + 2B_{1g} + A_{1g}$) of anatase phase were detected in all samples. It is worth noting that the strongest E_g mode (140 cm^{-1}) of *G*-TiO_{2-x} exhibits a blue shift and peak broadening compared with that of *B*-TiO_{2-x} and white TiO_2 (Figure 1g). It is well-known that the presence of many disorders would result in photons confinement effects and finally blue-shift and broadening of E_g mode [43], which are ascribed to crystal domain size and nonstoichiometry [44]. Thus, compared with those of *B*-TiO_{2-x} and white TiO_2, it is believed that the blue shift and linewidth increasing of E_g mode at ~140 cm^{-1} in *G*-TiO_{2-x} indicates the obvious change of TiO_2 lattice order during ultrasonication, which is in well agreement with HRTEM observation (Figure 1e-f). The chemical states of Ti and O atoms on the surface of *G*-TiO_{2-x} and *B*-TiO_{2-x} were further investigated by X-ray photoelectron spectroscopy (XPS). The shoulder peaks at ~457 eV in the Ti $2p_{3/2}$ and at 463 eV in Ti $2p_{1/2}$ XPS spectra, correlated with Ti^{3+}[45], can be obviously detected in the surface layer of *B*-TiO_{2-x} and *G*-TiO_{2-x} (Figure S4).

It is found that, compared with aqueous solution of *B*-TiO_{2-x}, aqueous solution of *G*-TiO_{2-x} shows a much enhanced NIR absorption (Figure 1h), especially around 920 nm (Figure S5), with the same Ti concentration, which can be ascribed to the change of TiO_{2-x} lattice order in *G*-TiO_{2-x}, as previously reported[46, 47].

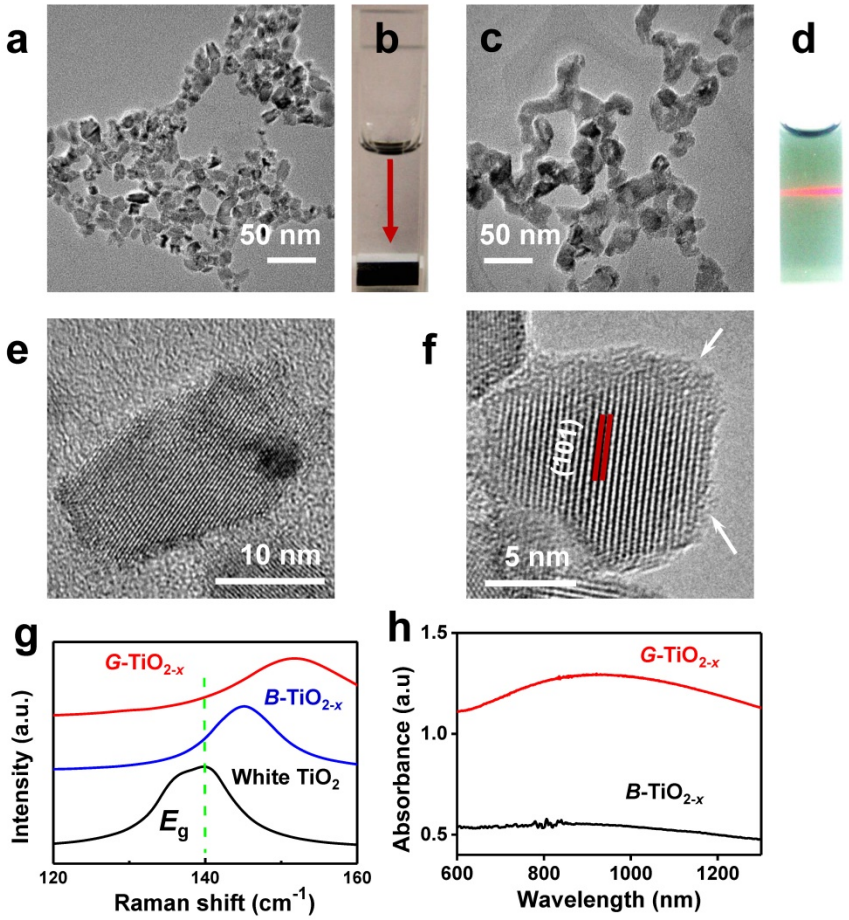

Figure 1. Representative TEM image of *B*-TiO_{2-x} (a) and its corresponding photograph of aqueous solution (b) (Ti concentration: 100 ppm). TEM image of *G*-TiO_{2-x} (c) and its corresponding photograph of aqueous solution (d) (Ti concentration: 100 ppm), the red beam of light came from a red laser pointer to indicate the excellent dispersity of *G*-TiO_{2-x}. HR-TEM images of *B*-TiO_{2-x} (e) and *G*-TiO_{2-x} (f), the arrows in (f) indicate the amorphous layer of TiO_{2-x}. (g) Raman spectra of white TiO_2, as-synthesized *B*-TiO_{2-x} and *G*-TiO_{2-x} at 140 cm^{-1}. (h) UV-vis absorbance spectra of aqueous solutions containing *B*-TiO_{2-x} and *G*-TiO_{2-x} at the same Ti concentration of 50 ppm.

PDT activity of *G*-TiO_{2-x}

The NIR laser-driven photocatalytic activity of *G*-TiO_{2-x} was further investigated by using 1,3-diphenylisobenzofuran (DPBF)[48], which is usually served as a singlet oxygen chemical probe for detection of ROS production. Basically, the optical absorption intensity of DPBF at 410 nm was measured by UV-Vis spectrum upon 980 nm laser irradiation, since the 980 nm continuous laser instrument is generally available and widely used than 920 nm laser instrument, and possesses lower energy and higher deep tissue penetration than that of 808 nm. The decay curves shown in **Figure 2**a clearly demonstrate that the groups of *G*-TiO_{2-x} alone, NIR laser irradiation alone and *G*-TiO_{2-x}+NIR are able to cause decrease in the absorption intensity of DBPF. Comparatively, much considerable decrease is observed in the presence of *G*-TiO_{2-x}+NIR, suggesting more ROS generation. To make more convincing, the ROS generation was further examined by electron spin resonance (ESR) methods [49], using 5,5-dimethyl-1-pyrolline-N-oxide (DMPO) as a spin trap agent. As shown in Figure 2b, the characteristic DMPO-OH spin adduct indicating the $OH^{\bullet}$ generation, is clearly found in the presence of *G*-TiO_{2-x}. More importantly, the intensity of DMPO-OH spin adduct significantly increases upon NIR laser irradiation, suggesting that *G*-TiO_{2-x} shows great potentials in NIR laser-driven PDT. Furthermore, confocal laser scanning microscopy (CLSM) was used to examine the photodynamic activity on HeLa cells. 2′,7′-dichlorodihydrofluorescein diacetate (DCFH-DA)[50], which is liable to be oxidized to strong green fluorescent 2′,7′-dichlorofluorescein (DCF) by ROS, was incubated with HeLa cells after different treatments. As expected, noticeable green fluorescence is observed in HeLa cells treated with *G*-TiO_{2-x}+NIR (Figure 2c_4), while could be hardly found in control cell groups including DMEM, *G*-TiO_{2-x} and NIR laser irradiation alone (Figure 2c_1-c_3). The quantified green fluorescent intensities of DCF from HeLa cell groups treated with *G*-TiO_{2-x}+NIR shows 6-7 folds higher than that of the aforementioned control cells groups (Figure 2d).

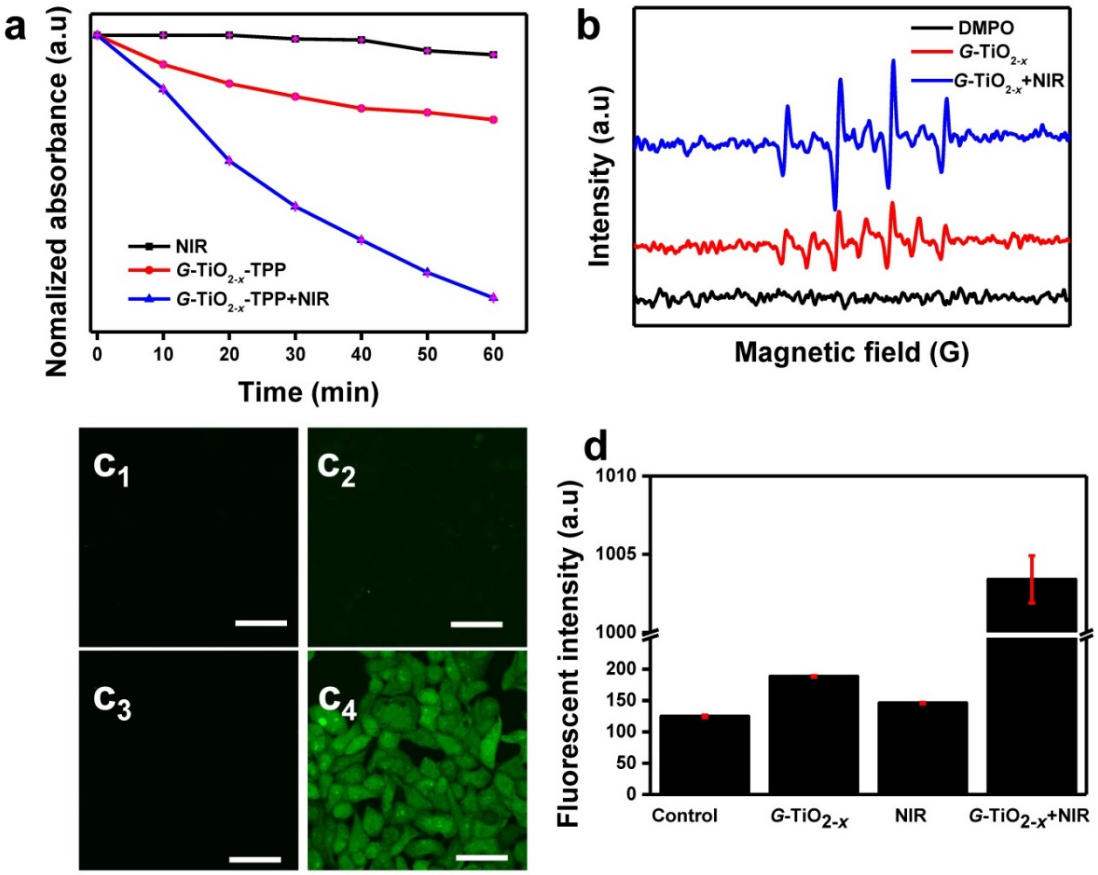

Figure 2. (a) Time-based absorption intensity (Mean±SD) reduction of DPBF after different treatments, monitored at 410 nm. (b) ESR spectra of different samples. (c)Confocal fluorescence images of HeLa cells stained by DCF-DA after different treatments: (c_1): without treatment as a control; (c_2): *G*-TiO_{2-x} incubation alone (Ti concentration: 50 ppm); (c_3): NIR laser irradiation alone for 5 min (980 nm, 0.72 W cm^{-2}); (c_4): *G*-TiO_{2-x}+NIR laser irradiation. All the scale bars in (c) are 50 μm. (d) The quantified green fluorescent intensities (Mean±SD) of ROS detection probe DCF from HeLa cell groups after aforementioned different treatments.

Photothermal effect of *G*-TiO_{2-x}

Encouragingly, upon 980 nm laser irradiation, the temperatures of solutions containing *G*-TiO_{2-x} gradually increase with concentrations (**Figure 3**a) and laser power densities (Figure S6a), whereas water as a control shows negligible temperature elevation, demonstrating *G*-TiO_{2-x} features an excellent photothermal effect and photostability (Figure S6b). To further explore the phototoxicity of *G*-TiO_{2-x} on HeLa cells, a standard 3-(4,5-dimethylthiazol-2-yl)-2,5-diphenyltetrazolium bromide (MTT) cell viability assay was performed on HeLa cells. After 24 h incubation without NIR laser irradiation, all the cell viabilities were over 85% even at a high concentration (the black histogram in Figure 3b), indicating *G*-TiO_{2-x} itself was nontoxic. However, upon 980 nm laser irradiation at a much lower power density of 0.72 W cm^{-2}, serve cell death occurred in the presence of *G*-TiO_{2-x} and the percentage of cell death shows dependence on concentrations (the red histogram in Figure 3b). In addition, the cells were stained by typan blue for visualization. As shown in Figure 3c, the dead cells are stained in blue (Figure $3c_4$), whereas the control cell groups including cells treated with Dulbecco's Modified Eagle Medium (DMEM), *G*-TiO_{2-x} and NIR alone remain unchanged (Figure $3c_1$-c_3). The phototoxicity of *G*-TiO_{2-x} could be further fluorescently visualized by CLSM. The cells treated with *G*-TiO_{2-x}+NIR show strong red fluorescence (Figure $3d_4$), originating from propidium iodine (PI) for dead cells. Comparatively, the aforementioned control cell groups display distinct green fluorescence (Figure $3d_1$-d_3), originating from calcein-AM (AM=acetoxymethyl) for live cells. All the results show that the *G*-TiO_{2-x} can serve as a single component photosensitizer for a single NIR laser-induced synergistic treatment of PDT and PTT.

Synthesis and characterization of *G*-TiO_{2-x}-TPP

It is well known that mitochondria are the vital energy center of cells and generally cause cell death through the generation of ROS, and the transportation of photosensitizers to mitochondria is unhindered, thus, mitochondria are preferred subcellular organelles for PDT. It is believed that the phototherapeutic efficacy could be highly improved

by constructing mitochondria-targeting photosensitizers for *in situ* production of ROS, since ROS generally suffer from short half-life (<40 ns) and limited diffusion distance (<20 nm), which significantly impede its capability to damage central cellular counterparts[51]. Therefore, the combination of mitochondria-targeted PDT/PTT could enable low dosage and low laser exposure accompanying with high phototherapeutic efficacy. Under this consideration, *G*-TiO_{2-x} was subsequently conjugated with TPP, which is a lipophilic cation selectively targeting to mitochondria, for mitochondria-targeted PDT/PTT. PEG terminated with amines at both terminals (NH_2-PEG_{5000}-NH_2) was used for the surface modification of *G*-TiO_{2-x}, thereinto, the formation of both the NH-O band[52] and the coordination bond between Ti atoms and amine groups [53] could improve the nanoparticles' dispersity and stability. Meanwhile, the other amine group terminal could be used for the TPP groups coupling through a carbodiimide reaction [54]. Aqueous solution of *G*-TiO_{2-x}-TPP shows a similar optical property in NIR region with *G*-TiO_{2-x}, and the absorbance around 920 nm is linearly enhanced with Ti concentrations (Figure S7). After surface modification, the hydrodynamic diameter of *G*-TiO_{2-x} increases from 59 to 135 nm after PEGylation, and to 196 nm after TPP conjugation (Figure S8a). The corresponding Zeta potential changes from -32.5 to -27 mV after PEGylation and 0.46 mV after TPP conjugation (Figure S8b). Besides the dynamic light scattering measurement, the Fourier Transform Infrared Spectroscopy (FTIR) was also characterized to indicate the successful PEG and TPP conjugation. In detail, the characteristic IR bands locating at 1384 cm^{-1} assigned to Ti–N–O vibrating band[55], and the FTIR displays a typical signal increase of ester band at 1725 cm^{-1} and benzene from 1600 to 1400 cm^{-1}[56] (Figure S9), respectively, confirming that PEG and TPP have been successfully conjugated onto the surface of *G*-TiO_{2-x}-TPP.

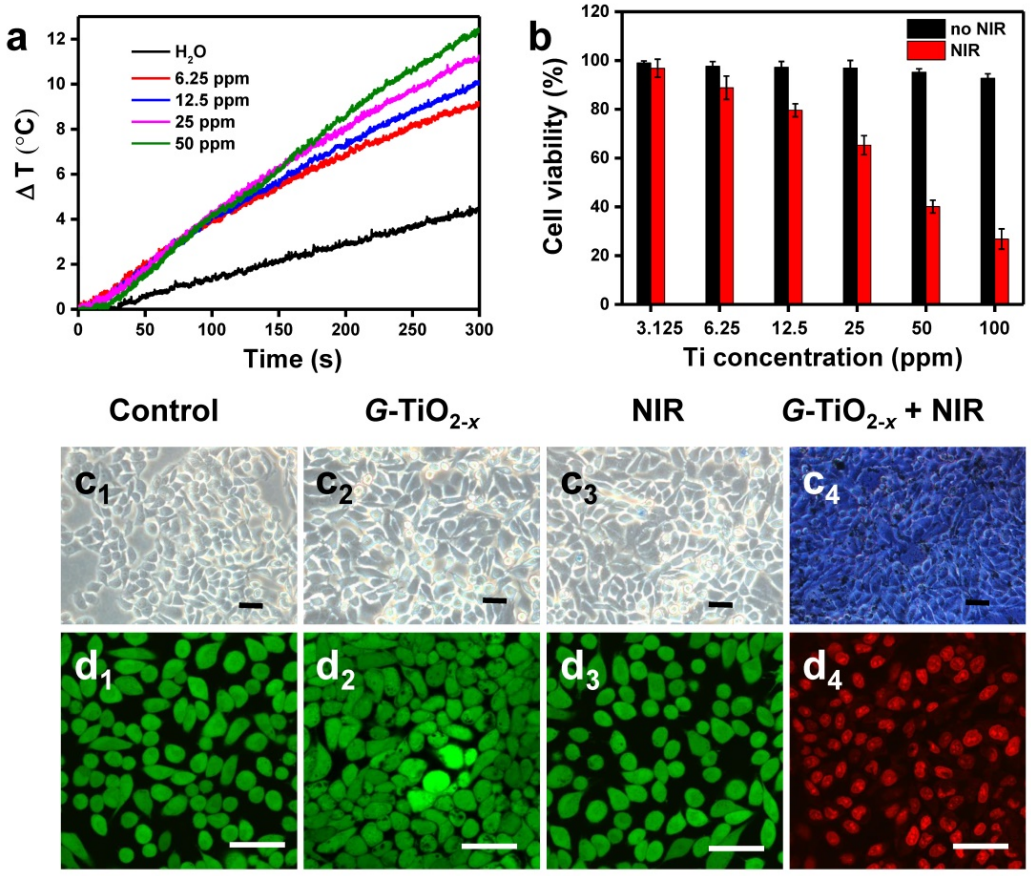

Figure 3. (a) Temperature evolution curves of pure water and aqueous solution containing *G*-TiO_{2-x} at different Ti concentrations under NIR laser irradiation for 5 min (980 nm, 0.72 W cm^{-2}). (b) *In vitro* cell viabilities (Mean±SD) of HeLa cells incubated with *G*-TiO_{2-x} at different Ti concentrations for 24 h without (the black histogram) and with NIR laser irradiation for 5 min (the red histogram, 980 nm, 0.72 W cm^{-2}). Optical microscopic images (c) of HeLa cells stained by trypan blue, and confocal fluorescence images of HeLa cells co-stained by calcein-AM and PI (d) after different treatments: (c_1-d_1): without treatment as a control; (c_2-d_2): *G*-TiO_{2-x} incubation alone (4 h, Ti concentration: 50 ppm); (c_3-d_3): NIR laser irradiation alone for 5 min (980 nm, 0.72 W cm^{-2}); (c_4-d_4): *G*-TiO_{2-x}+NIR laser irradiation (4 h, Ti concentration: 50 ppm, 980 nm, 0.72 W cm^{-2}). All the scale bars in (c-d) are 50 μm.

Intracellular localization of *G*-TiO_{2-x} and *G*-TiO_{2-x}-TPP

In order to evaluate the selective targeting efficacy of *G*-TiO_{2-x}-TPP to mitochondria, intracellular localization of *G*-TiO_{2-x} and *G*-TiO_{2-x}-TPP were investigated on HeLa cells by CLSM. After incubation with RITC-labeled *G*-TiO_{2-x} and *G*-TiO_{2-x}-TPP for 1 and 4 h, respectively, HeLa cells were stained with Mito-Tacker green (a mitochondria stain). It is found that both *G*-TiO_{2-x} and *G*-TiO_{2-x}-TPP can be taken up by HeLa cells, since the red channel is ascribed to the red fluorescence signal of RITC-labeled *G*-TiO_{2-x} and *G*-TiO_{2-x}-TPP (**Figure 4**a-b). Comparatively, much stronger red signals in HeLa cells incubated with *G*-TiO_{2-x}-TPP after 1 and 4 h indicate a higher cellular uptake efficiency of *G*-TiO_{2-x}-TPP than that of *G*-TiO_{2-x}, even after incubation with *G*-TiO_{2-x} for 4 h, which is further evidenced by the quantified red fluorescent intensities (Figure 4c). The green channel shows the location of mitochondria, and the yellow areas in merged pictures reveal the co-localization of green signal from Mito-Tracker green and red signal from FITC-labeled *G*-TiO_{2-x} and *G*-TiO_{2-x}-TPP. Negligible overlapping areas are observed in the cells incubated with *G*-TiO_{2-x} for 1 h, while weak yellow signals can be detected after incubation for 4 h, suggesting a part of *G*-TiO_{2-x} could be localized to mitochondria. Inspiringly, *G*-TiO_{2-x}-TPP is found to preferentially enter into mitochondria, which is revealed by the obvious and abundant yellow signals both after 1 and 4 h incubations, demonstrating *G*-TiO_{2-x}-TPP exhibits a higher selective localization to mitochondria than that of *G*-TiO_{2-x}, mainly attributing to the assistance of TPP ligand. The process of *G*-TiO_{2-x}-TPP targeting to mitochondria and subsequently inducing cell death are illustrated in Figure 4d.

In vivo blood circulation and biodistribution of *G*-TiO_{2-x}-TPP

Prior to *in vivo* cancer phototherapy, the blood circulation half-time and biodistribution of *G*-TiO_{2-x}-TPP was investigated. The Ti contents in blood and main tissues were determined by inductively coupled plasma-atomic emission spectrometry (ICP-AES) analysis. It is found that *G*-TiO_{2-x}-TPP exhibits a blood circulation half-life of 1 h (Figure S10a), which is considerably longer than organic molecules [57]. Similar to other nanoparticles, after 24 h intravenous injection, *G*-TiO_{2-x}-TPP was trend to be uptaken by reticuloendothelial system (RES) [58], including liver and spleen. About 2.6 ID%/g of *G*-TiO_{2-x}-TPP was accumulated within tumor mainly attributing to the enhanced permeability and retention (EPR) effect (Figure S10b) [59].

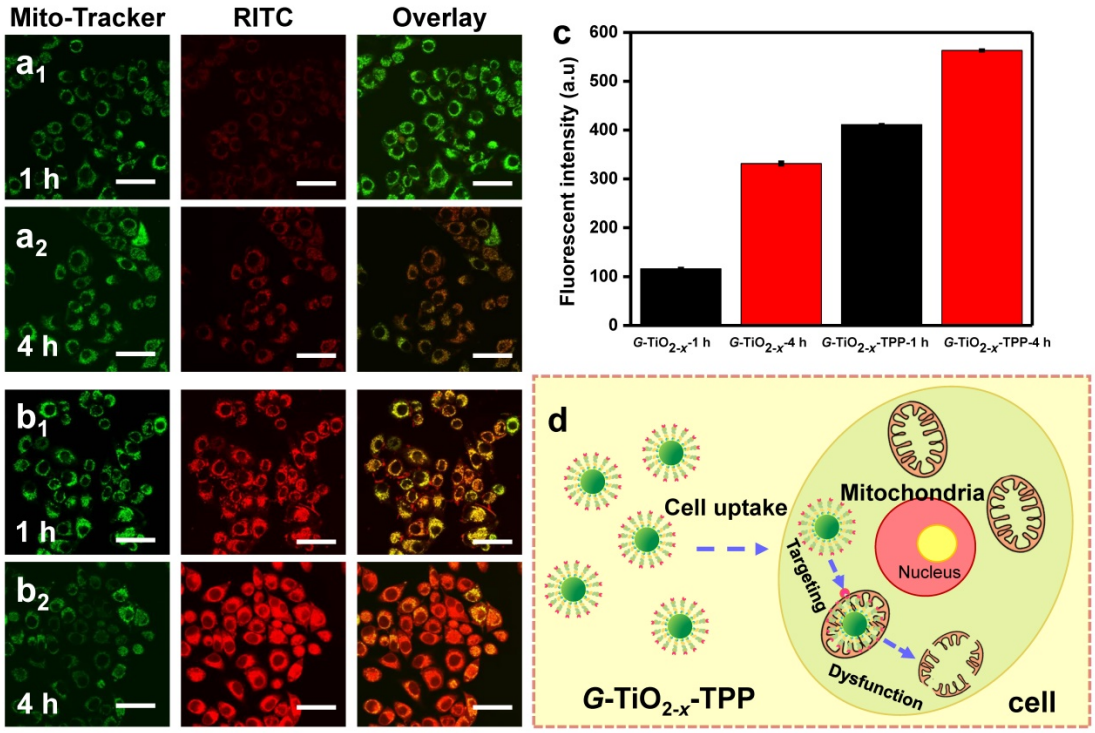

Figure 4. Confocal fluorescence microscopic images of HeLa cells treated with RITC-labeled *G*-TiO_{2-x} (a_1-a_2), and *G*-TiO_{2-x}-TPP (b_1-b_2) for 1 h and 4 h incubations, respectively, following by Mito-Tracker green stain. All the scale bars in (a-b) are 50 μm. The mitochondrial localization is evaluated by the co-localized fluorescence signal from Mito-Tracker green and RITC-labeled *G*-TiO_{2-x} and *G*-TiO_{2-x}-TPP. Yellow areas arising from the red and green signals denoted the co-localization of *G*-TiO_{2-x} and *G*-TiO_{2-x}-TPP within mitochondrial compartments. (c) The corresponding quantified fluorescent intensities (Mean±SD) of RITC-labeled *G*-TiO_{2-x} and *G*-TiO_{2-x}-TPP from HeLa cell groups after aforementioned different treatments. (d) Schematic illustration of the process of *G*-TiO_{2-x}-TPP targeting to mitochondria and subsequently inducing cell death.

In vivo PDT/PTT investigation

Furthermore, the *in vivo* phototherapeutic efficacy of *G*-TiO_{2-x}-TPP was investigated in detail. Mice bearing HeLa tumors on two flanks were randomly divided into two groups (n=6). Physiological saline containing *G*-TiO_{2-x}-TPP with a dosage of 8 mg kg^{-1} per mouse, which is relatively lower than that of Au nanorods (20 mg kg^{-1}) [60], was intravenously injected into the second group of mice. Then the left tumors were illuminated with a NIR laser at a much lower laser power density (980 nm, 0.72 W cm^{-2}), which is significantly lower than that of previously reported (20 W cm^{-2}) [61]. The local temperature changes of tumor site were real-time monitored by near-infrared thermal imaging instrument. The temperature of tumor treated with NIR laser irradiation alone just elevates to 38.8 °C (**Figure 5**a). Comparatively, the temperature of tumor treated with *G*-TiO_{2-x}-TPP+NIR elicits a faster and higher temperature elevation and increases to 55 °C (Figure 5b), which is sufficient to cause irreversible damages to cancer cells, after identical level of NIR laser illumination. As is expected, large areas of severe tissue damages, such as cellular destruction and apoptosis, were found in the histopathological analysis of tumor treated with *G*-TiO_{2-x}-TPP+NIR (Figure 5c_4). However, no obvious changes were found in control mice treated with physiological saline, NIR alone, and *G*-TiO_{2-x}-TPP alone (Figure 5c_1-c_3). Since *G*-TiO_{2-x}-TPP shows enhanced NIR absorption and high mitochondria-targeting efficiency, which ensures production of hyperthermia and ROS *in situ* for mitochondria targeted PTT/PDT, it is believed the mitochondria undergoes the combination mechanisms of both apoptosis and necrosis [62]. The phototherapeutic efficacy was further evaluated by measuring tumor growth rates. The tumors of mice treated with *G*-TiO_{2-x}-TPP+NIR show complete tumor elimination in the second day and no recurrence in the subsequent 18 days (Figure 5d), whereas the tumors of mice treated with physiological saline, *G*-TiO_{2-x}-TPP and NIR alone display sustainable growth, which could be further confirmed by the photographs of mice after different treatments in 18 days (Figure 5e). It is worth noting that, excellent phototherapeutic efficacy is achieved even at the relatively low tumor accumulation of *G*-TiO_{2-x}-TPP with a much lower laser power density and low dosage of *G*-TiO_{2-x}-TPP, mainly attributing to the successful mitochondria targeting and simultaneous and highly synergistic effect of PDT/PTT. All these results well demonstrate that such new kind of *G*-TiO_{2-x}-TPP with enhanced NIR absorption and mitochondria-targeting property can be employed as a desired photosensitizer for mitochondria-targeted phototherapy.

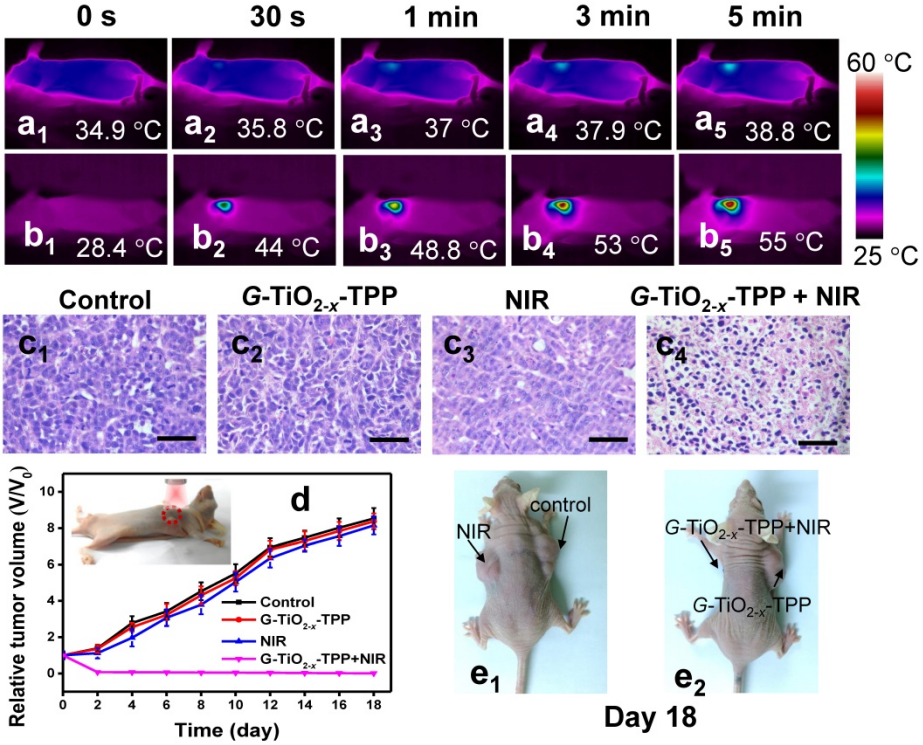

Figure 5. Infrared thermal images of nude mice bearing HeLa tumors after different treatments at varied time intervals: (a_1-a_5) NIR laser irradiation alone; (b_1-b_5) *G*-TiO_{2-x}-TPP+NIR laser irradiation for 5 min (980 nm, 0.72 W cm^{-2}). (c) H&E staining of tumor sections collected from the groups of mice upon different post treatments: (c_1) saline; (c_2) *G*-TiO_{2-x}-TPP alone (8 mg kg^{-1}, per mouse); (c_3) NIR laser irradiation alone; and (c_4) *G*-TiO_{2-x}-TPP+NIR laser irradiation. (d) Tumor growth curves of different groups of tumors-bearing mice. The inset shows photograph of cancer phototherapy. (e) Photographs of mice in 18 days post-treatment. All the scale bars in (c) are 50 μm.

In vitro and *in vivo* toxicity investigation

Since nanoparticles are liable to accumulate within liver, kidney and potential harmful to brain, three types of normal cells including rat liver cells (BRL), renal tubular duct epithelial cells of rat (NRK-52E) and brain capillary endothelial cells (BCECs) were incubated with *G*-TiO_{2-x}-TPP at varied Ti concentrations for the cytotoxicity investigation. The cell viability was assessed by a standard MTT assay. After 24 incubation, it is found that no obvious cytotoxicity of *G*-TiO_{2-x}-TPP is observed, which can be evidenced by the percentages of cell viabilities of all the three types were above 85% (Figure S11a) and no significant cells morphologies changes (Figure S11c-e), indicating *G*-TiO_{2-x}-TPP is biocompatible to liver, kidney and brain. In addition, two types of brain-related cancer cells, including human glioblastoma cells (U87MG) and rat adrenal pheochromocytoma cell line (PC12), which were generally used to study the diseases of brain, were further incubated with *G*-TiO_{2-x}-TPP for evaluating the cytotoxicity of *G*-TiO_{2-x}-TPP on brain in detail. As is expected, the results of MTT assays on these two types of cancer cells show that *G*-TiO_{2-x}-TPP exhibites negiligible cytoxicity (Figure S11b, f-g), demonstrating *G*-TiO_{2-x}-TPP is safe to brain.

Furthermore, *in vivo* biocompatibility investigation was conducted in detail. The mice after intravenous injection of *G*-TiO_{2-x}-TPP were euthanized at predetermined time points (*i.e.*, 3, 15, 30 days). The blood and main organs were acquired for hemanalysis and histological analysis, respectively. No disorder is observed in the hematological and biochemical parameters (Figure S12a-p). And the main tissues (including heart, liver, spleen, lung, kidney) show no abnormity from the Hematoxylin and Eosin (H&E) staining results (Figure S13), indicaiting that *G*-TiO_{2-x}-TPP is hemo/histocompatible. Moreover, the brain tissue sections of cortex, hippocampus and striatum were also collected and stained with H&E to investigate the potential *in vivo* brain toxicity. It is found that the aforementioned brain tissues still retained the similar morphologies in 3, 15, 30 days after intravenous injection of *G*-TiO_{2-x}-TPP (Figure S14), which was compared with the control groups, demonstrating that *G*-TiO_{2-x}-TPP has negligible side effects to brain. All the results have shown that *G*-TiO_{2-x}-TPP is highly biocompatible for further biomedical application.

Conclusion

In this study, we have demonstrated a simple but effective approach to develop a new kind of stable *G*-TiO_{2-x} from *B*-TiO_{2-x} by a subsequently strong ultrasonication. The aqueous solution of *G*-TiO_{2-x} exhibits an obvious green color and enhanced NIR absorption, especially around 920 nm, which is mainly ascribed to the change of TiO_{2-x} lattice order, as can be found in the obvious thickness increasement of amorphous layer of *G*-TiO_{2-x}. Attributing to the significant enhancement in NIR absorption, excellent NIR laser-induced PDT and PTT activity of *G*-TiO_{2-x} has been obtained. In addition, in order to further reduce the laser power density to minimize potential damages to healthy tissues, *G*-TiO_{2-x} was subsequently conjugated with TPP ligand for mitochondria-targeted PDT/PTT. Both *in vitro* and *in vivo* results well demonstrated the excellent mitochondria-targeting capability and high phototherapeutic efficacy of *G*-TiO_{2-x}-TPP, under a single NIR laser irradiation at a much lower power density (980 nm, 0.72 W cm^{-2}) and low intravenous injection dosage (8 mg kg^{-1} per mouse). Moreover, *G*-TiO_{2-x} is proved to have high hemo/histrocompatibility for further biological application. The successful construction of mitochondria-targeted simultaneous and synergistic PDT/PTT based on such a new kind of *G*-TiO_{2-x} overcomes the traditional drawbacks of combinatorial treatment of PTT/PDT, such as overdose of nanomaterials and UV light exposure, and exhibits highly improved phototherapeutic efficacy and safety as well as biocompatibility, providing new strategies for future precise minimal/non-invasive tumor treatment.

Supplementary Material

Supplementary figures.
http://www.thno.org/v07p1531s1.pdf

Acknowledgements

This work was supported by the China National Funds for Distinguished Young Scientists (51225202), National Natural Science Foundation of China (Grant No. 51132009), Shanghai Excellent Academic Leaders Program (14XD1403800).

Competing Interests

The authors have declared that no competing interest exists.

References

1. Loo C, Lowery A, Halas N, West J, Drezek R. Immunotargeted nanoshells for integrated cancer imaging and therapy. Nano Lett. 2005; 5: 709-11.
2. Dolmans DEJGJ, Fukumura D, Jain RK. Photodynamic therapy for cancer. Nat Rev Cancer. 2003; 3: 380-7.
3. Chen Q, Chen H, Shapiro H, Hetzel FW. Sequencing of combined hyperthermia and photodynamic therapy. Radiat Res. 1996; 146: 293-7.
4. Gottfried V, Kimel S. Temperature effects on photosensitized processes. J Photochem Photobiol B. 1991; 8: 419-30.

5. Kuo W-S, Chang Y-T, Cho K-C, Chiu K-C, Lien C-H, Yeh C-S, et al. Gold nanomaterials conjugated with indocyanine green for dual-modality photodynamic and photothermal therapy. Biomaterials. 2012; 33: 3270-8.
6. Kuo W-S, Chang C-N, Chang Y-T, Yang M-H, Chien Y-H, Chen S-J, et al. Gold nanorods in photodynamic therapy, as hyperthermia agents, and in near-infrared optical imaging. Angew Chem. 2010; 122: 2771-5.
7. Lin J, Wang S, Huang P, Wang Z, Chen S, Niu G, et al. Photosensitizer-loaded gold vesicles with strong plasmonic coupling effect for imaging-guided photothermal/photodynamic therapy. ACS Nano. 2013; 7: 5320-9.
8. Sahu A, Choi WI, Lee JH, Tae G. Graphene oxide mediated delivery of methylene blue for combined photodynamic and photothermal therapy. Biomaterials. 2013; 34: 6239-48.
9. Tian B, Wang C, Zhang S, Feng L, Liu Z. Photothermally enhanced photodynamic therapy delivered by nano-graphene oxide. ACS Nano. 2011; 5: 7000-9.
10. Yin ZF, Wu L, Yang HG, Su YH. Recent progress in biomedical applications of titanium dioxide. Phys Chem Chem Phys. 2013; 15: 4844-58.
11. Gratzel M. Photoelectrochemical cells. Nature. 2001; 414: 338-44.
12. Chen X, Mao SS. Titanium dioxide nanomaterials: synthesis, properties, modifications, and applications. Chem Rev. 2007; 107: 2891-959.
13. Yu Z, Pan W, Li N, Tang B. A nuclear targeted dual-photosensitizer for drug-resistant cancer therapy with NIR activated multiple ROS. Chem Sci. 2016; 7: 4237-44.
14. Kubo W, Tatsuma T. Detection of H2O2 released from TiO2 photocatalyst to air. Analy Sci. 2004; 20: 591-3.
15. Murakami Y, Kenji E, Nosaka AY, Nosaka Y. Direct detection of OH radicals diffused to the gas phase from the UV-irradiated photocatalytic TiO2 surfaces by means of laser-induced fluorescence spectroscopy. J Phys Chem B. 2006; 110: 16808-11.
16. Nosaka Y, Nakamura M, Hirakawa T. Behavior of superoxide radicals formed on TiO2 powder photocatalysts studied by a chemiluminescent probe method. Phys Chem Chem Phys. 2002; 4: 1088-92.
17. Miyoshi N, Kume K, Tsutumi K, Fukunaga Y, Ito S, Imamura Y, et al. Application of titanium dioxide (TiO2) nanoparticles in photodynamic therapy (PDT) of an experimental tumor. AIP Conf Proc. 2011; 1415: 21-3.
18. Kotagiri N, Sudlow GP, Akers WJ, Achilefu S. Breaking the depth dependency of phototherapy with Cerenkov radiation and low-radiance-responsive nanophotosensitizers. Nat Nanotech. 2015; 10: 370-9.
19. Smith AM, Mancini MC, Nie S. Bioimaging: Second window for in vivo imaging. Nat Nanotech. 2009; 4: 710-1.
20. König K. Multiphoton microscopy in life sciences. J Microsc. 2000; 200: 83-104.
21. George S, Pokhrel S, Ji Z, Henderson BL, Xia T, Li L, et al. Role of Fe doping in tuning the band gap of TiO2 for the photo-oxidation-induced cytotoxicity paradigm. J Am Chem Soc. 2011; 133: 11270-8.
22. Asahi R, Morikawa T, Ohwaki T, Aoki K, Taga Y. Visible-light photocatalysis in nitrogen-doped titanium oxides. Science. 2001; 293: 269-71.
23. Asahi R, Morikawa T, Irie H, Ohwaki T. Nitrogen-doped titanium dioxide as visible-light-sensitive photocatalyst: designs, developments, and prospects. Chem Rev. 2014; 114: 9824-52.
24. Zuo F, Wang L, Wu T, Zhang Z, Borchardt D, Feng P. Self-doped Ti3+ enhanced photocatalyst for hydrogen production under visible light. J Am Chem Soc. 2010; 132: 11856-7.
25. Mao C, Zuo F, Hou Y, Bu X, Feng P. In situ preparation of a Ti3+ self-doped TiO2 film with enhanced activity as photoanode by N2H4 reduction. Angew Chem Int Ed. 2014; 53: 10485-9.
26. Justicia I, Ordejón P, Canto G, Mozos JL, Fraxedas J, Battiston GA, et al. Designed self-doped titanium oxide thin films for efficient visible-light photocatalysis. Adv Mater. 2002; 14: 1399-402.
27. Chen X, Liu L, Yu PY, Mao SS. Increasing solar absorption for photocatalysis with black hydrogenated titanium dioxide nanocrystals. Science. 2011; 331: 746-50.
28. Wang Z, Yang C, Lin T, Yin H, Chen P, Wan D, et al. H-doped black titania with very high solar absorption and excellent photocatalysis enhanced by localized surface plasmon resonance. Adv Funct Mater. 2013; 23: 5444-50.
29. Yang C, Wang Z, Lin T, Yin H, Lü X, Wan D, et al. Core-shell nanostructured "black" rutile titania as excellent catalyst for hydrogen production enhanced by sulfur doping. J Am Chem Soc. 2013; 135: 17831-8.
30. Mou J, Lin T, Huang F, Chen H, Shi J. Black titania-based theranostic nanoplatform for single NIR laser induced dual-modal imaging-guided PTT/PDT. Biomaterials. 2016; 84: 13-24.
31. Ren W, Yan Y, Zeng L, Shi Z, Gong A, Schaaf P, et al. A near infrared light triggered hydrogenated black TiO2 for cancer photothermal therapy. Adv Healthcare Mater. 2015; 4: 1526-36.
32. Lo JH, von Maltzahn G, Douglass J, Park J-H, Sailor MJ, Ruoslahti E, et al. Nanoparticle amplification via photothermal unveiling of cryptic collagen binding sites. J Mater Chem B. 2013; 1: 5235-5240.
33. Zhang L, Tian Q, Xu W, Kuang X, Hu J, Zhu M, et al. Construction of 980 nm laser-driven dye-sensitized photovoltaic cell with excellent performance for powering nanobiodevices implanted under the skin. J Mater Chem. 2012; 22: 18156-63.
34. Jung HS, Han J, Lee J-H, Lee JH, Choi J-M, Kweon H-S, et al. Enhanced NIR radiation-triggered hyperthermia by mitochondrial targeting. J Am Chem Soc. 2015; 137: 3017-23.
35. Han K, Lei Q, Wang SB, Hu JJ, Qiu WX, Zhu JY, et al. Dual-stage-light-guided tumor inhibition by mitochondria-targeted photodynamic therapy. Adv Funct Mater. 2015; 25: 2961-71.
36. Yu Z, Sun Q, Pan W, Li N, Tang B. A near-infrared triggered nanophotosensitizer inducing domino effect on mitochondrial reactive oxygen species burst for cancer therapy. ACS Nano. 2015; 9: 11064-74.
37. Willis WT, Jackman MR, Bizeau ME, Pagliassotti MJ, Hazel JR. Hyperthermia impairs liver mitochondrial function in vitro. Am J Phys REGI. 2000; 278: R1240-6.
38. Wang Z, Cai F, Chen X, Luo M, Hu L, Lu Y. The role of mitochondria-derived reactive oxygen species in hyperthermia-induced platelet apoptosis. PLoS One. 2013; 8: e75044.
39. Murphy MP. Targeting lipophilic cations to mitochondria. Biochim Biophys Acta (BBA) - Bioenerg. 2008; 1777: 1028-31.
40. Wang Z, Yang C, Lin T, Yin H, Chen P, Wan D, et al. Visible-light photocatalytic, solar thermal and photoelectrochemical properties of aluminium-reduced black titania. Energy Environ Sci. 2013; 6: 3007-14.
41. Hasan Nia M, Rezaei-Tavirani M, Nikoofar AR, Masoumi H, Nasr R, Hasanzadeh H, et al. Stabilizing and dispersing methods of TiO2 nanoparticles in biological studies. J Paramed Sci. 2015; 6: 96-105.
42. Pan S, Liu X, Guo M, Yu Sf, Huang H, Fan H, et al. Engineering the intermediate band states in amorphous Ti3+-doped TiO2 for hybrid dye-sensitized solar cell applications. J Mater Chem A. 2015; 3: 11437-43.
43. Parker JC, Siegel RW. Raman microprobe study of nanophase TiO2 and oxidation-induced spectral changes. J Mater Res. 1990; 5: 1246-52.
44. Li Bassi A, Cattaneo D, Russo V, Bottani CE, Barborini E, Mazza T, et al. Raman spectroscopy characterization of titania nanoparticles produced by flame pyrolysis: The influence of size and stoichiometry. J Appl Phys. 2005; 98: 074305-9.
45. Fu Y, Du H, Zhang S, Huang W. XPS characterization of surface and interfacial structure of sputtered TiNi films on Si substrate. Mater Sci Eng A. 2005; 403: 25-31.
46. Chen X, Liu L, Liu Z, Marcus MA, Wang W-C, Oyler NA, et al. Properties of disorder-engineered black titanium dioxide nanoparticles through hydrogenation. Sci Rep. 2013; 3: 1-7.
47. Naldoni A, Allieta M, Santangelo S, Marelli M, Fabbri F, Cappelli S, et al. Effect of nature and location of defects on bandgap narrowing in black TiO2 nanoparticles. J Am Chem Soc. 2012; 134: 7600-3.
48. Carloni P, Damiani E, Greci L, Stipa P, Tanfani F, Tartaglini E, et al. On the use of 1,3-diphenylisobenzofuran (DPBF). Reactions with carbon and oxygen centered radicals in model and natural systems. Res Chem Intermed. 1993; 19: 395-405.
49. Moan J, Wold E. Detection of singlet oxygen production by ESR. Nature. 1979; 279: 450-1.
50. Bourré L, Thibaut S, Briffaud A, Rousset N, Eléouet S, Lajat Y, et al. Indirect detection of photosensitizer ex vivo. J Photochem Photobiol. 2002; 67: 23-31.
51. Robertson CA, Evans DH, Abrahamse H. Photodynamic therapy (PDT): A short review on cellular mechanisms and cancer research applications for PDT. J Photochem Photobiol. 2009; 96: 1-8.
52. Hanawa T. A comprehensive review of techniques for biofunctionalization of titanium. J Periodontal Implant Sci. 2011; 41: 263-72.
53. Yuan LS, Efendi J, Razali NSH, Nur H. Fine-tuning the local structure and catalytic activity of titanium-amine functionalized silica in oxidation of limonene by aqueous hydrogen peroxide. Catal Commun. 2012; 20: 85-8.
54. Wang X-H, Peng H-S, Yang L, You F-T, Teng F, Tang A-W, et al. Poly-l-lysine assisted synthesis of core-shell nanoparticles and conjugation with triphenylphosphonium to target mitochondria. J Mater Chem B. 2013; 1: 5143-52.
55. Yang G, Jiang Z, Shi H, Xiao T, Yan Z. Preparation of highly visible-light active N-doped TiO2 photocatalyst. J Mater Chem. 2010; 20: 5301-9.
56. Martins AF, de Oliveira DM, Pereira AGB, Rubira AF, Muniz EC. Chitosan/TPP microparticles obtained by microemulsion method applied in controlled release of heparin. Int J Biol Macromol. 2012; 51: 1127-33.
57. McMurry TJ, Parmelee DJ, Sajiki H, Scott DM, Ouellet HS, Walovitch RC, et al. The effect of a phosphodiester linking group on albumin binding, blood half-life, and relaxivity of intravascular diethylenetriaminepentaacetato aquo gadolinium(III) MRI contrast agents. J Med Chem. 2002; 45: 3465-74.
58. Nie S. Understanding and overcoming major barriers in cancer nanomedicine. Nanomedicine (London, England). 2010; 5: 523-8.
59. Maeda H, Wu J, Sawa T, Matsumura Y, Hori K. Tumor vascular permeability and the EPR effect in macromolecular therapeutics: a review. J Control Release. 2000; 65: 271-84.
60. Maltzahn Gv, Park J-H, Agrawal A, Bandaru NK, Das SK, Sailor MJ, et al. Computationally guided photothermal tumor therapy using long-circulating gold nanorod antennas. Cancer Res. 2009; 69: 3892-900.
61. Huang X, El-Sayed IH, Qian W, El-Sayed MA. Cancer cell imaging and photothermal therapy in the near-infrared region by using gold nanorods. J Am Chem Soc. 2006; 128: 2115-20.
62. Oleinick NL, Morris RL, Belichenko I. The role of apoptosis in response to photodynamic therapy: what, where, why, and how. Photochem Photobiol Sci. 2002; 1: 1-21.